Modeling and design of an energy-efficient dual-motor actuation unit with a planetary differential and holding brakes

Verstraten, Tom; Furnémont, Raphaël Guy; Lopez Garcia, Pablo; Rodriguez Cianca, David; Cao, Hoang-Long; Vanderborght, Bram; Lefeber, Dirk

Published in:
Mechatronics

DOI:
10.1016/j.mechatronics.2017.12.005

Publication date:
2018

Document Version:
Accepted author manuscript

Modeling and design of an energy-efficient dual-motor actuation unit with a planetary differential and holding brakes

Tom Verstraten[a,*], Raphaël Furnémont[a], Pablo Lopez-Garcia[a], David Rodriguez-Cianca[a], Hoang-Long Cao[a], Bram Vanderborght[a], Dirk Lefeber[a]

[a] *All authors are with the Robotics and Multibody Mechanics Research Group (R&MM), Vrije Universiteit Brussel, Pleinlaan 2, 1050 Elsene. The R&MM Research Group is a partner of Flanders Make.*

Abstract

By connecting two drivetrains to a single load, a redundant degree of freedom is created. In this work, we investigate how the redundancy of such a system can be exploited in order to make it more energy efficient. The system under study consists of two drivetrains coupled to a planetary differential. Both drivetrains are composed of a geared DC motor and a holding brake. First, we derive an accurate semi-empirical model of this system and prove its validity on a test setup. Based on this model, which includes nonlinear friction terms, we analyze how the power flows and energy losses depend on the redundant degree of freedom. Furthermore, we discuss how the design of the actuator can be optimized for energy efficiency. This strategy is applied to a case study, where a 250W geared DC motor is replaced by a more efficient dual-motor actuator. Experiments confirm that a dual-motor actuator succeeds in reducing the energy consumption at various loads and speeds. We also show that the results are very sensitive to friction and other speed- and load-dependent losses.

Keywords: Actuators; energy efficiency; redundant systems; over-actuated systems; planetary differential; epicyclic gears

1. Introduction

In most applications, motors drive a load at a constant speed and a constant torque, i.e. in steady-state conditions. In this case, the motor can be designed to obtain the highest efficiency for this specific working point. Typical tasks in robotics, however, require the motors to operate at varying speeds and varying loads. The efficiency of the motor changes with speed and torque [1], and may therefore be used very inefficiently throughout the motion [2][3]. This situation

*Corresponding author. E-mail: Tom.Verstraten@vub.be

can be improved by coupling a second motor to the load, resulting in an additional - redundant - degree of freedom. The actuator's redundancy can then be exploited to distribute the power requirements among both motors, such that they are used in a more energy-efficient way overall. Such concepts, especially when combined with energy buffers, have great potential in biomedical applications such as exoskeletons and prosthetics. Sugar and Holgate, for example, suggested variable transmissions as a way of shaping a motor's speed-torque curve to the biological ankle profile [4]. Combining variable transmissions with a series spring [5][6] or a flywheel [7] also holds great promise in terms of energy efficiency. Aló et al. studied the possibility of using an Infinitely Variable Transmission (IVT) with flywheel in a knee actuator [8] and found that such a concept could potentially reduce the actuator's energy requirement by 85% in walking. Finally, Variable Impedance Actuators (VIAs) can also be classified as overactuated systems with energy buffers. They typically consist of two motors, one of which is used to regulate the stiffness or pretension of a spring. VIAs have been studied extensively in recent years, and many concepts have been proposed by various groups. For an extensive overview, we refer to the review paper by Vanderborght et al. [9].

The simplest way of creating redundancy is arguably to couple multiple motors to the same driveshaft. This is essentially a parallel arrangement, where the output torque is the sum of both motor-gearbox torques, creating *static redundancy*. Statically redundant actuators are probably the simplest embodiment of an over-actuated system, and have been investigated by several authors [10][11][12][13][14]. Morrell et al. proposed to combine a small and a large motor, the former directly coupled to the load and the latter through a compliant transmission [15]. Later, the concept was refined by also optimizing the location of the actuators in a robotic arm, an approach called "Distributed Macro-Mini actuation" [16]. The idea behind the control is that the large motor applies of low-frequency torques, while the smaller motor corrects for high-frequency disturbances. This approach has several advantages, including improved backdrivability, better small-signal force control and position control bandwidth, reduced forces during impacts, and improved dynamic range.

Another option is to couple motors to a differential. In this case, one obtains a *kinematically redundant actuator*, where the output speed can be higher than that of a single motor-gearbox. Different types of differentials can be chosen to couple the motors. In robotics, the most extensively studied concepts are based on single-stage planetary differentials. The concept was first introduced by Ontañon-Ruiz with the aim of reducing stiction [17]. Later, Kim et al. [18, 19], proposed to use the second motor to control the impedance of the actuator. Lee and Choi [20] explored the possibility of shaping the actuator's operating range more favorably than that of a regular motor. And lastly, Girard et al. developed control strategies that can be applied to these types of actuators [21, 22, 23]. One may, of course, devise more complex drivetrains to enhance the actuator's capabilities. Babin et al. [24], for example, took the concept a step further by not grounding both motors, but instead mounting one of them to a movable component. Gao et al. suggested using a two-stage gearbox as a differential

mechanism [25]. There are numerous possibilities, but actuators with a single-stage planetary differential stand out because of their simplicity, making them very suitable for fundamental research and the testing of control strategies.

So far, analyses in literature have been limited to linearized approximations where friction is neglected. This work is the first to present a semi-empirical model of a dual-motor actuator which includes (nonlinear) friction. Using the model as a basis, we demonstrate the concept's potential in terms of energy efficiency, and assess how the required power should be distributed among the motors in order to obtain the highest energy efficiency. The main contributions of this work are the model itself and the extensive analysis of how the design and power distribution can be tuned in order to reduce minimize the actuator's energy consumption. Furthermore, the accuracy and reliability of the model is verified in experiments, and the energy efficiency of the design is validated by comparing the proposed dual-motor actuator to an equivalent geared DC motor. Our results show that friction and other load- and speed-dependent losses, which were not considered in other works, have a strong influence on the design and control of multi-motor actuators.

The paper is structured as follows. First, we derive the model of the actuator (Section 2). We analyze its electrical power consumption and discuss how the design can be optimized to obtain a high energy efficiency (Section 3). Theoretical conclusions are supported by a case study, where a 250W geared DC motor is replaced by a more energy-efficient dual-motor alternative (Section 4). This case study is then validated by measurements on an actual test bench (Section 5), with special attention for the differences between theory and practice. Finally, the results are discussed in Section 6, and conclusions are presented in Section 7.

2. Equations

2.1. Concept

A regular single-stage planetary gearbox consists of a sun gear, a ring gear, planetary gears and a carrier. In order to achieve the highest gear ratio, the sun is typically used as the input and the carrier as output, while the ring is grounded. By using the ring as an additional input, however, the planetary gearbox can be turned into a planetary differential. This component is the basis of the dual-motor actuator presented in this work. The basic schematic of the dual-motor actuator (DMA) is shown in Fig. 1. Two input drivetrains are coupled to the sun and ring gear of a planetary differential, while, just like in a regular planetary gear, the output is coupled to the carrier. As shown in Table 1, this topology offers the highest reductions between the inputs and the output. As a result, the reductions offered by the planetary differential are exploited in the best possible way, leading to the most efficient design in terms of space.

The input drivetrains each consist of a motor and gearbox with a holding brake. When it is engaged, the motor can be switched off, such that no electrical power is consumed. An additional advantage is that the brakes can hold higher

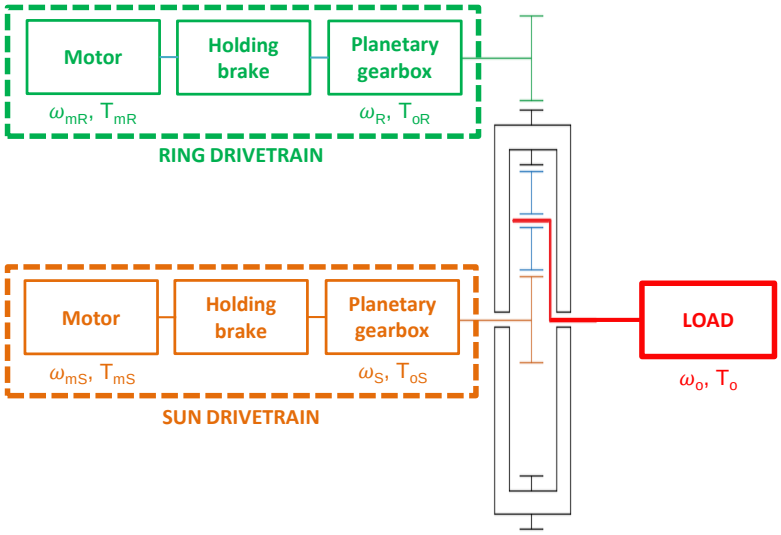

Figure 1: Dual-motor actuator setup. The actuator consists of two drivetrains, coupled to the ring and sun gear of a planetary differential. The load is coupled to the carrier gear, just like in an ordinary planetary gear. Holding brakes, placed in between the motors and their gearboxes, can be controlled to lock the position of the drivetrain, upon which the motor can be switched off.

torques than the motor, which is limited by the maximum current it can provide. Without brakes or any other locking mechanism, the maximum torque that can be provided by the actuator would be determined by the weakest motor, as we will explain in section 2.3. Having a locking mechanism is therefore essential in order to make the actuator's operating range as large as possible.

Previously presented concepts have used a cam-based clutch [18] or worm gears [20][24] as locking devices. Worm gears can be designed such that they lock when backdriven, without any need for actuation. With worm gears on both branches, however, the entire actuator becomes non-backdrivable. This makes the actuator less suitable for robotics applications where, in many cases, backdrivability is desired. For this reason, we used controllable brakes instead of worm gears, like in Girard et al. [21]. The brakes are positioned on the motor shafts, rather than directly on the ring and sun gears. The main advantage of of this approach is that the required braking torque is scaled down through the gearbox, such that a smaller brake can be used.

2.2. Design equations

A schematic of the DMA, along with definitions of the torques T and speeds ω, is given in Fig. 2. The signs of the torques and speeds follow the passive sign convention [26], i.e. input powers $T_S\omega_S$ and $T_R\omega_R$ are positive, while output power $T_o\omega_o$ is negative.

Inputs	Output	Kinematic relationship
Sun, ring	Carrier	$\omega_o = \frac{1}{1+\rho}\omega_S + \frac{\rho}{1+\rho}\omega_R$
Sun, carrier	Ring	$\omega_o = \frac{1+\rho}{\rho}\omega_C - \frac{1}{\rho}\omega_S$
Ring, carrier	Sun	$\omega_o = (1+\rho)\,\omega_C - \rho\omega_R$

Table 1: Kinematic relationships for different configurations of a planetary differential. The output speed is denoted by ω_o, carrier speed by ω_C, sun speed by ω_S and ring speed by ω_R. The planetary differential ratio ρ is defined in Eq. (4). For a single-stage planetary differential, $1 < \rho \leq 9$. In this case, a configuration where the sun and ring gear are used as inputs yields the highest overall reduction.

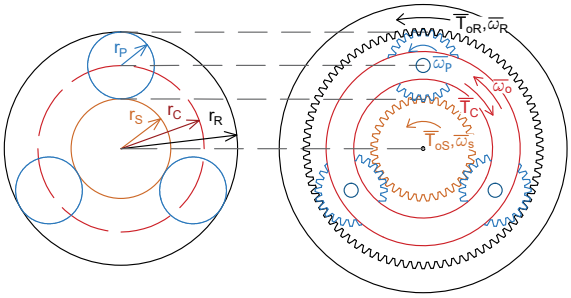

Figure 2: Planetary differential with definitions of torque and speed. Definitions respect the passive sign convention.

The actuator has one static and two kinematic degrees of freedom (DoF). The static degree of freedom is defined as the number of independent shaft torques that are needed to satisfy the static equilibrium conditions; the kinetic degree of freedom is defined as the number of independent speeds that fully determine the motion of the differential [27]. Imposing a certain motion to a load imposes one static and one kinematic DoF. Consequently, the mechanism is statically determined, but is still left with one redundant kinematic DoF. In other words, we will be able to choose the way how both motors contribute to the output speed while – in steady state – their torques are completely determined by the output torque.

2.2.1. Speeds

The ring and sun drivetrains consist of a geared DC motor. We can thus write

$$\omega_{m\lambda} = n_\lambda \omega_\lambda \tag{1}$$

where n_λ ($\lambda = R, S$) are the gear ratios of the planetary gearboxes in the ring and sun drivetrain, respectively. Because of the redundant kinematic DoF, the ring motor angular velocity ω_{mR} and the sun motor angular velocity ω_{mS} can be chosen independently. We define the *speed ratio* i as

$$i = \frac{\omega_R}{\omega_S} = \frac{\omega_{mR}/n_R}{\omega_{mS}/n_S} \tag{2}$$

The speed ratio i is the degree of freedom which we would like to control, in such a way that the most energy-efficient operation is achieved. The velocity ω_o of the carrier, which serves as the output, is a linear combination of the sun and ring motor velocities. From Table 1, we find that this relationship is given by

$$\omega_o = \frac{1}{1+\rho}\omega_S + \frac{\rho}{1+\rho}\omega_R \tag{3}$$

where we defined the *planetary differential ratio* ρ as

$$\rho = \frac{r_R}{r_S} \tag{4}$$

This ratio is related to the gear ratio with locked ring n_{PG} (i.e. the differential is used as an ordinary planetary gearbox) by

$$\rho = n_{PG} - 1 \tag{5}$$

Geometry dictates that $r_R > r_S$, so $\rho > 1$.

Combining Eqs. (2) and (3), we can write the input speeds of the planetary differential as a function of the output speed:

$$\begin{bmatrix} \omega_{mS} \\ \omega_{mR} \end{bmatrix} = \begin{bmatrix} \frac{n_S(1+\rho)}{1+\rho i} \\ \frac{n_R(1+\rho)i}{1+\rho i} \end{bmatrix} \omega_o \tag{6}$$

2.2.2. Torques

2.2.2.1. Differential torques. Consider the planetary differential displayed in Fig. 2. We assume that all friction is caused by the meshing of the gear teeth. If both sun and ring are delivering power to the planets, i.e.

$$T_{oS}\left(\omega_S - \omega_o\right) > 0 \tag{7}$$

$$T_{oR}\left(\omega_R - \omega_o\right) > 0 \tag{8}$$

the meshing efficiency for the planets with the sun (η_{SP}) and the ring (η_{RP}) can be found by dividing the output power by the input power:

$$\eta_{SP} = \frac{-T_P^{(S)}\left(\omega_P - \omega_o\right)}{T_{oS}\left(\omega_S - \omega_o\right)} \tag{9}$$

$$\eta_{RP} = -\frac{T_P^{(R)}\left(\omega_P - \omega_o\right)}{T_{oR}\left(\omega_R - \omega_o\right)} \tag{10}$$

in which T_{oS} and T_{oR} are the torques on the sun and ring gear, and $T_P^{(S)}$ and $T_P^{(R)}$ are the torques on the planets due to meshing with the sun and ring gear, respectively. In the above equations, the speeds with which we multiply the torques are relative to the carrier, as if it is fixed. Indeed: if the sun or ring gear is not moving with respect to the carrier, the gear teeth will not move with

respect to each other, and there will be no power transfer. Also note that, if one of the conditions (7) or (8) is false, the nominator and denominator need to be reversed in the corresponding equation (9) or (10).

The torque balance is given by

$$T_{oS} + T_{oR} = T_C \tag{11}$$

and the power balance, in a reference frame attached to the rotating carrier, by

$$\eta_{SP} T_{oS} \left(\omega_S - \omega_C\right) + \eta_{RP} T_{oR} \left(\omega_R - \omega_o\right) = 0 \tag{12}$$

Note that we could also have found this equation by stating the power equilibrium in a single planetary gear, i.e.

$$T_P^{(S)} \left(\omega_P - \omega_C\right) = T_P^{(R)} \left(\omega_P - \omega_o\right) \tag{13}$$

Indeed, with a fixed carrier and zero planetary inertia, the only powers through the planetary gears are the powers accepted from the ring and sun.

Inserting the speed equation (3) into Eq. (12), we find (after some small calculations)

$$\eta_{SP} T_{oS} \rho - \eta_{RP} T_{oR} = 0 \tag{14}$$

Combining this with Eq. (11), we find the relationship between the torque on the carrier (output) and the sun and ring torques:

$$T_C = \left(\rho \frac{\eta_{SP}}{\eta_{RP}} + 1\right) T_{oS} \tag{15}$$

$$T_C = \left(\frac{1}{\rho} \frac{\eta_{RP}}{\eta_{SP}} + 1\right) T_{oR} \tag{16}$$

The speed equation (3) shows that the output speed is a linear combination of the ring and sun speed with positive coefficients. In other words, the output speed is a weighted average of the sun and ring speed, and will lie somewhere in between these speeds. Furthermore, T_{oS}, T_{oR} and T_{oC} are defined in such a way that they always have the same sign. Combining these two facts, we can easily see that

$$sign\left[T_{oS}\left(\omega_S - \omega_o\right)\right] = -sign\left[T_{oR}\left(\omega_R - \omega_o\right)\right] \tag{17}$$

It is therefore sufficient to check only one of the two conditions (7) and (8); if one is false, the other one is true. As a result, η_{RP} and η_{SP} will appear as a product in all equations, regardless of which power flow case we are in. We can thus define $\eta_{PG} = \eta_{RP}\eta_{SP}$ and write

$$T_C = \left(\rho \eta_{PG}^{sign[T_C(\omega_S - \omega_o)]} + 1\right) T_{oS} \tag{18}$$

$$T_C = \left(\frac{1}{\rho} \eta_{PG}^{sign[T_C(\omega_R - \omega_o)]} + 1\right) T_{oR} \tag{19}$$

To further simplify the equations, we define the efficiency function C_{PG} of the planetary differential:

$$C_{PG} = \eta_{PG}^{sign[T_C(\omega_S - \omega_o)]} \tag{20}$$

and rewrite it as a function of i:

$$C_{PG} = \eta_{PG}^{sign\left[\frac{1-i}{1+\rho i} T_C \omega_o\right]} \tag{21}$$

With this function,we can write the relationship between the carrier torque T_C and the sun and ring torques T_{oS} and T_{oR} as

$$T_C = (\rho C_{PG} + 1)\, T_{oS} \tag{22}$$

$$T_C = \left(\frac{1}{\rho C_{PG}} + 1\right) T_{oR} \tag{23}$$

Eqs. (22) and (23) demonstrate that the torques on the ring and sun gear are fully determined by the required output. Furthermore, by combining them, we can find

$$T_{oR} = \rho C_{PG} T_{oS} \tag{24}$$

indicating that, by design, the torque in the ring branch will be higher than that in the sun branch.

2.2.2.2. Motor torques. The relationships between the motor torques $T_{m\lambda}$ and the torques on the sun or ring gear of the planetary differential $T_{o\lambda}$ are given by

$$T_{m\lambda} = B_\lambda(\omega_o, T_o) \cdot \left[\frac{C_\lambda}{n_\lambda} T_{o\lambda} + T_{C\lambda} sign(\omega_{m\lambda}) + \nu_\lambda \omega_{m\lambda}\right] \tag{25}$$

where we introduced a friction torque composed of Coulomb and viscous friction, with friction coefficients $T_{C\lambda}$ (Coulomb friction) and ν_λ(viscous friction). C_R and C_S represent the efficiency function of the gearbox, defined as

$$C_\lambda = \eta_\lambda^{-sign(T_{o\lambda}\omega_\lambda)} \tag{26}$$

where η_λ represents the catalog efficiency of the respective gearbox. The torque on the motor shaft is multiplied by the braking function $B_\lambda(\omega_o, T_o)$, defined as

$$B_\lambda(\omega_o, T_o) = \begin{cases} 0 & \text{(brake engaged)} \\ 1 & \text{(brake disengaged)} \end{cases} \tag{27}$$

By combining motor equation (25) with torque equations (22) and (23), we obtain

$$T_{mS} = B_S(\omega_o, T_o) \cdot \left[\frac{C_S}{n_S} \frac{1}{1+\rho C_{PG}} T_C + T_{CS} sign(\omega_{mS}) + \nu_S \omega_{mS}\right] \tag{28}$$

$$T_{mR} = B_R(\omega_o, T_o) \cdot \left[\frac{C_R}{n_R} \frac{\rho C_{PG}}{1+\rho C_{PG}} T_C + T_{CR} sign(\omega_{mR}) + \nu_R \omega_{mR}\right] \tag{29}$$

Furthermore, the losses between the carrier and the output, which are mostly due to bearings, can be modeled by a combination of Coulomb friction and viscous friction, leading to the following equation for the output torque:

$$T_o = T_C - T_{CC} sign(\omega_o) - \nu_C \omega_o \tag{30}$$

2.2.3. Electrical

The following model can be applied to find the motor currents I_λ:

$$I_\lambda = \frac{1}{k_{T\lambda}} T_{m\lambda} \tag{31}$$

In this equation, $k_{T\lambda}$ represents the torque constant of the respective motor. Furthermore, motor voltages U_λ can be calculated with

$$U_\lambda = k_{T\lambda}\omega_{m\lambda} + R_\lambda I_\lambda \tag{32}$$

with R_λ the winding resistance of the motor. The electrical powers $P_{elec,\lambda}$ are given by

$$P_{elec,\lambda} = U_\lambda \cdot I_\lambda \tag{33}$$

Finally, the total electrical power P_{elec} consumed by the actuator is simply the sum of both motor powers:

$$P_{elec} = P_{elec,S} + P_{elec,R} \tag{34}$$

Here, we neglect the power consumed by the brakes. Whether this assumption is justified, depends entirely on the type of brake that is being used. Bi-stable brakes, for example, do not consume any energy while they are engaged or disengaged; energy input is only required to change their state [28]. If the application requires the brake to switch only sporadically between its engaged and disengaged state, such a bi-stable brake will indeed consume a negligible amount of power. In other cases, novel concepts such as statically balanced brakes [29] and electroadhesive clutches [30] can be used to hold the drivetrain's position at a low energy cost.

2.3. Constraints and limitations

Any drivetrain is subject to electrical and mechanical limitations. In this section, we discuss how these affect the design of a DMA.

2.3.1. Maximum speed

Typically, a maximum speed is specified on the datasheets of the motor and gearbox. Denoting the maximum motor speeds by $\omega_{mS,max}$ (sun) and $\omega_{mR,max}$ (ring), we find that the maximum achievable output speed $\omega_{o,max}$ is given by (dual-motor operation)

$$\omega_{o,max} = \frac{1}{1+\rho}\left(\frac{\omega_{mS,max}}{n_S} + \rho\frac{\omega_{mR,max}}{n_R}\right) \tag{35}$$

Inherently, the ring branch will thus contribute more to the output speed.

2.3.2. Maximum torque

The output torque is limited by several factors. The maximum motor and gearbox torque, as specified by the manufacturer, must be respected in order to avoid damage or reduced lifetime of the components. Furthermore, the maximum output current of the controller's power stage may also limit the achievable torque. We will denote the maximum torque that can be provided by the motors, regardless of its cause, with $T_{S,max}$ and $T_{R,max}$ for the sun and ring branch, respectively. The maximum torque that can be delivered by the actuator then depends on its operation mode of the actuator. When one of the branches is locked (single-motor operation), the maximum output torque is fully determined by the active branch. If the active branch is the sun, we obtain a maximum output torque $T_{o,max,S}$ given by

$$T_{o,max,S} = (\rho C_{PG} + 1) \frac{n_S}{C_S} T_{S,max} \tag{36}$$

For the ring, the maximum output torque $T_{o,max,R}$ is

$$T_{o,max,R} = \left(\frac{1}{\rho C_{PG}} + 1 \right) \frac{n_R}{C_R} T_{R,max} \tag{37}$$

In dual-motor operation, both branches are active at the same time. While their speeds can be controlled independently, their torques cannot; they are fully determined by the required output torque, as shown by Eqs. (22) and (23). As a consequence, the weakest branch effectively limits the output torque. The maximum output torque in dual-motor operation, $T_{o,max,D}$, can thus be written as

$$T_{o,max,D} = min\left[T_{o,max,S}; T_{o,max,R}\right] \tag{38}$$

In order to maximize the dual-motor operating region, where redundancy can be exploited, the gear ratios must therefore be chosen such that $T_{o,max,S} = T_{o,max,R}$. This yields

$$\frac{n_S}{n_R} = \frac{1}{\rho C_{PG}} \frac{C_S}{C_R} \frac{T_{R,max}}{T_{S,max}} \tag{39}$$

If similar or identical motors are used, and neglecting the efficiency of the planetary differential, we find

$$\frac{n_S}{n_R} = \frac{1}{\rho} \tag{40}$$

Consequently, in order to get the most out of the dual-motor operation, the ring branch will need to deliver higher torques at lower speeds compared to the sun branch. Nevertheless, it might be interesting to make one branch stronger than the other. Such a design would result in an actuator which can deliver high torques at low speeds, as well as high speeds at low torques. Certain applications, such as actuated ankle prosthetics, could benefit from such an actuator design [4].

2.3.3. Maximum voltage

The motor voltage U_λ cannot exceed the voltage $U_{\lambda,max}$ available from the power source:

$$|U_\lambda| < U_{\lambda,max} \tag{41}$$

According to Eq. 32, the motor voltage links the motor torque to the motor speed. Hence, Eq. (41) limits the output speed that can be achieved at certain output torque.

3. Theoretical discussion

3.1. Maximum achievable efficiency

Since energy consumption is the integral of electrical power over time, the high-power operating points can be expected to have the largest influence on the overall energy consumption. Fortunately, motors and gearboxes tend to operate close to their maximum efficiency when they are delivering high powers. Maximizing the maximum efficiency of the actuator is therefore a first step towards maximizing the overall efficiency of the actuator.

To simplify the problem, the maximum efficiency of the sun and ring branch will be defined as η_{Sb} and η_{Rb}. This efficiency includes the motor and gearbox losses, as well as friction losses. Defining the efficiency function of each branch as

$$C_{\lambda b} = \eta_{\lambda b}^{-sign(T_{o\lambda}\omega_\lambda)} \tag{42}$$

the electrical power can be written as

$$P_{elec} = C_{Rb} T_{mR} \omega_{mR} + C_{Sb} T_{mS} \omega_{mS} \tag{43}$$

The strong relationship between the motor's Joule losses and the square of the current is not represented by this simplified equation. It therefore does not account for the high losses suffered by a motor delivering a low torque or, in the extreme case, a static torque. Nevertheless, the simplification allows us to draw some interesting conclusions about the relationship between the design and the maximum efficiency that can be achieved. After some small calculations, and neglecting losses in the planetary differential and on the output shaft, Eq. (43) can be rewritten as a function of the output torque and speed:

$$P_{elec} = \left(C_{Rb} \frac{\rho i}{1+\rho i} + C_{Sb} \frac{1}{1+\rho i} \right) T_o \omega_o \tag{44}$$

When both motors are in forward drive, we can write this equation as

$$\eta_{tot} = \frac{T_o \omega_o}{P_{elec}} = \frac{1+\rho i}{\left(\frac{\rho i}{\eta_{Rb}} + \frac{1}{\eta_{Sb}} \right)} \tag{45}$$

As expected, the efficiency of the actuator depends on the speed ratio i. The optimal speed distribution puts the most power demand on the branch with the

most efficient drivetrain. A high speed ratio, for example, corresponds to a high ring speed and, consequently, high power in the ring branch. Eq. (45) shows that, in this case, the ring branch efficiency dominates the overall efficiency. Note that the planetary gear radius ratio ρ and the speed ratio i appear in couples ρi. This suggests that the parameter ρ – values typically between 1 and 9 for a one-stage planetary geartrain – is not that important, because it can to some extent be corrected by the speed ratio i. However, ρ also has a significant influence on the torques and speeds that need to be delivered by the motors, and consequently on the gearbox choice. A high ρ corresponds to a high planetary differential reduction, leading to a decreased need for high gearbox reductions on the sun and ring motor. Considering that smaller gearbox reductions are, in general, more efficient [31], a higher ρ may allow for a more efficient design of the separate branches. As we will see in section 4.1, this improves the overall efficiency of the actuator as well.

Eq. (45) also shows one very important property of the DMA design: the efficiency in dual-motor operation can never be higher than that of the most efficient branch. This means that, if the actuator is intended to replace a conventional motor with gear reducer, this will only be an improvement in terms of energy consumption if at least one of both branches can be made more energy-efficient than the initial motor-gearbox combination.

Finally, if both drives are identical, i.e. $\eta_{Rb} = \eta_{Sb} = \eta$, the maximum efficiency becomes

$$\eta_{tot} = \eta \tag{46}$$

In other words, with identical drives, the design of the planetary gear nor the speed ratio influence the maximum achievable efficiency of the actuator.

3.2. Power flows

In a conventional geared motor, the imposed motion and the friction losses determine the power required from the motor. For overactuated systems such as the DMA, the user can choose how to distribute the powers over both motors. To do this in an energy-efficient way is not a straightforward task, because the internal power flows have a strong influence on the gear losses inside the actuator. The power flows that may occur can be divided into eight types, as shown in Fig. 3. Which type of power flow occurs, depends on two things: the direction in which power is transferred to the load, as well as the speed ratio. Interestingly, positive power at the output does not necessarily imply that both input motors are delivering positive power as well. For values of $i < 0$, one motor is motoring (positive power flow), while the other is regenerating (negative power flow). This has important implications for the design and control of the actuator, because the power flows influence the efficiency function of the planetary differential and the planetary gearboxes in both branches. The values of the efficiency functions C_S, C_R and C_{PG} are listed in the figure for each of the power flow types.

The transitions between the different power flow types shown in Fig. 3 deserve special interest, because each corresponds to a specific way of using the actuator.

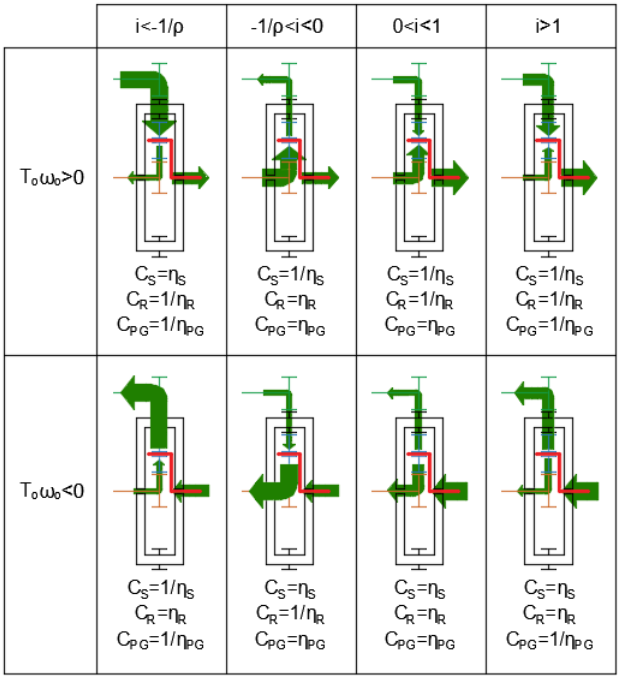

Figure 3: Possible power flows in a DMA configuration based on a planetary differential. The power flows are represented by green arrows, where wider arrows represent higher powers. There are eight types of power flow, all of which can be characterized by the output power $T_o\omega_o$ and the speed ratio i. The values of the efficiency functions C_S, C_R and C_{PG} depend on the power flow type; their values are listed for each of the eight cases.

- The extreme case of $i = \infty$ corresponds to zero speed of the sun branch. At zero speed, friction losses are eliminated, and the only remaining losses are the Joule losses[1] in the motor. These can also be eliminated by engaging a locking device, if is available on the branch.

- At $i = 1$, the sun, ring and carrier move at exactly the same angular velocities ($\omega_S = \omega_R = \omega_o$). This type of motion is known as "block motion" [32]. The efficiency function C_{PG}, given by Eq. (21), becomes

$$C_{PG} \quad = \quad \eta_{PG}^{sign(0)} = 1 \tag{47}$$

  Meshing losses are completely eliminated, because the gear teeth of the planets no longer move with respect to those of the sun and the ring.

- At $i = 0$, the ring branch is standing still. By engaging a locking device,

[1] These are the losses due to heating of the motor windings. They are also known by other names, such as copper losses, Ohmic losses, resistive losses, armature winding losses, etc.

the losses in this branch can be eliminated completely, just like in the $i = \infty$ case.

- For a speed ratio $i = -1/\rho$, both input branches may turn at a certain speed, but will nonetheless combine to an output speed of zero. Obviously, this type of operation is not very efficient for stationary applications. The better option is to lock both branches, such that they can deliver a reaction torque which combines to the required output torque.

4. Case study: replacing a 250W drivetrain

In this section, a reference drivetrain (a 250W Maxon RE65 DC motor with 51:1 planetary gearbox) is replaced by a more energy efficient dual-motor actuator design. In order to make both designs comparable, we will attempt to shape the DMA's operating range in such a way that it resembles that of the 250W motor. We chose to work with a Maxon 150W RE40 DC motor, which is one of the most efficient in Maxon's catalog, and combine it with a 90W Maxon RE35 DC motor. In terms of size, this is the smallest combination of motors that is able to span the same operating range as the 250W motor. The parameters of these motors, as well as those of the reference motor, are listed in Table 2. The motors of the DMA are equipped with planetary gearboxes from the Maxon GP42 range, which fits both motors. The gear ratios are chosen in such a way that the DMA covers most of the reference drivetrain's operating range. If similar solutions are available, the most energy efficient solution is used. Finally, since the friction coefficients are unknown, we will assume $T_{CC} = 0$, $\nu_C = 0$, $T_{CR} = 0$, $T_{CS} = 0$ and $T_{Cref} = 0$. All friction is assumed to present itself as viscous friction in the sun and ring branch. As suggested in [33], the corresponding friction coefficients are derived from the motors' no-load speed and no-load current:

$$\nu_\lambda = \frac{k_{T\lambda} I_{nl\lambda}}{\omega_{nl\lambda}} \tag{48}$$

With this formula, we obtain friction coefficients ν_S = 5.2E-6 Nm/(rad/s), ν_R = 6.1E-6 Nm/(rad/s) and ν_{ref} = 8.9E-5 Nm/(rad/s).

4.1. Energy-efficient design

Table 3 shows several DMA solutions which cover a similar operating range as the reference drivetrain. In this table, two critical design parameters are varied: the gear ratio of the planetary differential and the placement of the two motors. Except for design 2, all designs lead to a higher efficiency than the reference drivetrain. The highest gains in efficiency occur for ρ=9. A high ρ will allow to decrease the gear ratio of the sun drivetrain and increase the ring drivetrain gear ratio, as predicted by (39). Decreasing the gear ratio of a planetary gearbox is particularly interesting if it leads to a reduction of the number of gearbox stages, since this will greatly improve gearbox efficiency. Indeed, the gearboxes in the sun branch in designs 3 and 4 (ρ=9) have one stage less compared to designs 1 and 2 (ρ=1.5), resulting in much higher gearbox

	Maxon RE65	Maxon RE40	Maxon RE35
Nominal power	250 W	150 W	90 W
Nominal speed	3710 rpm	6940 rpm	7000 rpm
Nominal torque T_{max}	485 mNm	177 mNm	101 mNm
Max. speed ω_{max}	3000 rpm	12000 rpm	12000 rpm
No-load speed ω_{nl}	3960 rpm	7580 rpm	7740 rpm
No-load current I_{nl}	665 mA	137 mA	169 mA
Max. efficiency η_{max}	83%	91%	86%
Terminal resistance R	0.0821 Ohm	0.299 Ohm	0.583 Ohm
Torque constant k_t	55.4 mNm/A	30.2 mNm/A	19.4 mNm/A
Speed constant k_b	172 rpm/V	317 rpm/V	328 rpm/V
Mass m	2100 g	480 g	340 g

Table 2: Parameters of the Maxon motors used in this section.

	DMA Ring			DMA Sun			Differential		Efficiency	
	P_{nom}	n_R	η_R	P_{nom}	n_S	η_S	ρ	η_{PG}	mean	max.
Design 1	150 W	113	72%	90 W	113	72%	1.5	94%	59%	67%
Design 2	90 W	156	72%	150 W	66	72%	1.5	94%	48%	64%
Design 3	150 W	126	72%	90 W	26	81%	9	94%	61%	68%
Design 4	90 W	216	72%	150 W	15	81%	9	94%	63%	71%
Reference drivetrain (Maxon RE65 250W, 51:1 reduction)									51%	64%

Table 3: Overview of DMA designs and their performance. Efficiencies (calculated with the equations presented in Section 2) depend on both speed and torque. The mean efficiency is taken over the entire range of torques and speeds that can be achieved with the actuator; the maximum efficiency is the highest efficiency over the entire operating range.

efficiencies η_S. As a result, these high-ρ designs also result in a better overall efficiency. A high value of ρ can thus be considered as a must for an energy-efficient dual-motor design.

The placement of the ring and sun motor is a more difficult subject, because it is closely related to the way the operating range is shaped – something which can be influenced through the choice of the gear ratios of both drivetrains and the way the holding brakes are used. In this regard, Eq. (24) can again serve as an important guideline. Knowing that the sun branch can easily be made efficient because it benefits more from the reduction offered by the planetary differential, it makes sense to exploit this branch as much as possible in single-motor operation. This means that the operating range of the sun motor must be maximized, which can be accomplished by choosing a motor with high nominal power. In Table 3, design 4, where the 150W motor is used in the sun branch, is indeed the most efficient.

4.2. Weight, volume and operating range

Reducing energy consumption was the main goal of the optimization. Nevertheless, volume and weight can also be reduced by a dual-motor architecture.

	Weight	Volume
Reference drive	**5.8 kg**	**1.13 dm^3**
Dual-motor actuator	**2.6 kg**	**0.512 dm^3**
Ring drive	0.62 kg	0.145 dm^3
Sun drive	0.94 kg	0.186 dm^3
Differential	1.0 kg	0.180 dm^3

Table 4: Estimated weight and volume of the reference drive and the dual-motor actuator, based on the datasheets of off-the-shelf components (i.e., the combined weight of the motor, gearbox and brake). The structure to hold the dual-motor actuator is not included in this calculation, so the estimated weight and volume can be considered as a lower bound. The additional weight can, however, be compensated to some extent by eliminating parts of the separate off-the-shelf components through an integrated design.

The estimated weights and volumes for the reference drivetrain and the DMA are shown in Table 4. The weight and volume of the reference drivetrain are almost twice as high as those of the DMA. Even though the estimated weight does not account for the weight of the structure, there appears to be a lot of margin for adding components. An integrated design, which combines the reductions of the individual motors and the planetary differential in a single housing, can also lead to a considerable reduction in weight and volume [21]. The width of the DMA will, however, tend to be larger than that of the single-motor equivalent. The sum of the diameters of the DMA's composing drivetrains is 84 mm, while the reference drivetrain has a diameter of 81 mm.

Also important to note is that we designed the DMA to match the operating range of a conventional drivetrain. Several applications in robotics, however, do not require high speeds at high torques and, consequently, do not use the full operating range of the motor [4]. One of the main advantages of the DMA is that its operating range can be turned into an L-shape, i.e. with a high-speed low-torque region and a high-torque low-speed region [20]. Interestingly, these are exactly the regions in which a DC motor is inefficient [1]. With an L-shaped operating range, the DMA can be optimized for operation in these regions, pushing up the efficiency to even higher values. Furthermore, by eliminating the unused part of the operating range, the DMA can be composed of smaller motors, reducing the overall size and weight [21].

To summarize, the analysis in this work already shows the potential of a dual-motor design compared to a regular motor with gear reducer. However, the benefits in terms of efficiency, weight and compactness can only be fully unlocked when the design, and more specifically the operating range, is optimized for a specific application.

4.3. Efficiency maps

In previous work [1], we introduced efficiency maps as a tool to visualize an actuator's torque- and speed-dependent efficiency in its entire operating region. Figure 4 shows the efficiency maps of the two most energy-efficient designs, designs 3 and 4, and the reference drivetrain. As predicted in section 4.1, the

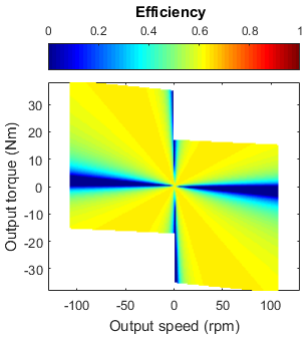

(a) Reference drivetrain.

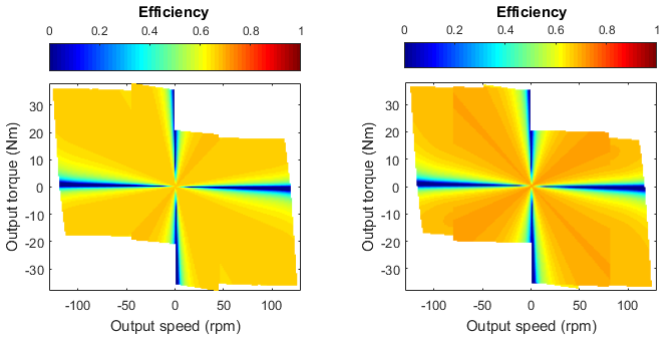

(b) DMA (design 3). (c) DMA (design 4).

Figure 4: Efficiency maps of (a) the reference drivetrain, (b) dual-motor actuator design 3 and (c) dual-motor actuator design 4, according to Table 3. The white areas denote combinations of speed and torque which cannot be delivered by the actuator, because at least one of the constraints listed in section 2.3 is violated. The dual-motor actuator has a higher efficiency over a broad range, and performs particularly better at low torques.

efficiency maps of design 3 and 4 are comparable, although the average efficiency of design 4 is clearly higher. Comparing the DMA designs to the reference drivetrain, the DMA not only has a higher maximum efficiency, but is also able to operate close to its maximum efficiency in a larger part of its operating range. Furthermore, the DMA is much more efficient than the reference motor at low powers. This is where the losses in the drivetrain have the highest impact, because they are high relative to the total output power. In fact, when an actuator is backdriven by the load, it may still need to deliver energy if the actuator's energy losses are higher than the energy flowing in from the load [1]. In Fig. 4, this type of operation is characterized by an efficiency of zero, which corresponds to the dark blue zones at high-torque low-speed and high-speed low-torque. A large part of the reference motor's operating range consists of such zero-efficiency regions. The DMA, however, is much more efficient in these areas. To understand why, we have to look at the operating modes of the actuator.

4.4. Operating modes and speed ratio i

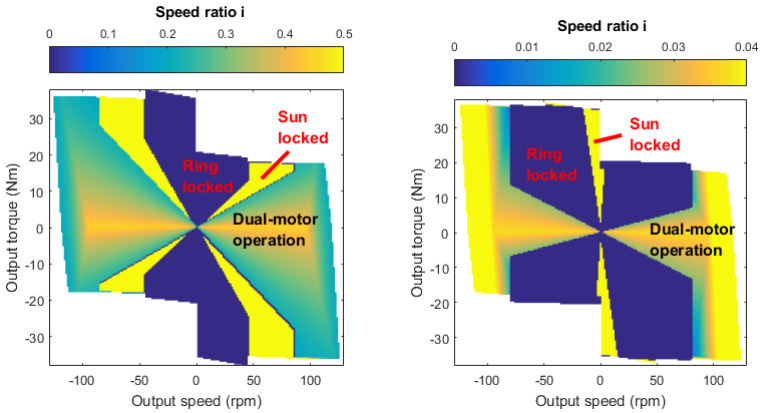

(a) Design 3. (b) Design 4.

Figure 5: Optimal operating modes and speed ratios i for designs 3-4, as specified in Table 3. Dark blue denotes single-motor operation with locked ring (i=0); yellow denotes single-motor operation with locked sun ($i = \infty$). In dual-motor operation, the speed ratio is shown. The white areas denote combinations of speed and torque which cannot be delivered by the actuator, because at least one of the constraints listed in section 2.3 is violated. Dual-motor operation is preferred when the required output torque is low compared to the required speed. At high torques and low speeds, single-motor operation is a more efficient choice. For these specific designs, a locked ring is preferable over a locked sun. This applies especially to design 4.

Energy-efficient operation of the DMA depends on two crucial elements: a good choice of the operating mode (dual-motor or single-motor operation) and, in dual-motor operation, a well-selected speed ratio. The optimal speed ratio i and the brake functions $B_\lambda\left(\omega_o, T_o\right)$ complement each other[2], and can be mapped together as a function of torque and speed. Such maps are shown in Fig. 5, for designs 3 and 4 from Table 3.

For both designs, single-motor operation covers a large part of the operating range. In this case, all power will be provided by the unlocked drivetrain. If this drivetrain can be made highly efficient, very high efficiencies can be obtained in single-motor operation. This explains the success of design 4, which, as illustrated by the large blue regions in Fig. 5, strongly exploits single-motor operation by locking the ring branch.

It appears that dual-motor operation becomes interesting when the demanded torque is low w.r.t. the demanded speed. In dual-motor operation, the speeds can be distributed over both motor branches, significantly lowering the viscous friction losses. At low torques and high speeds, the Joule losses

[2] As we explained in section 3.2, the usage of the brakes can be related to the speed ratio. Locking the ring branch corresponds to a speed ratio of $i = 0$, while braking the sun branch corresponds to $i = \infty$.

(proportional to torque squared) and the gearbox losses (proportional to the power flow) are less crucial than the viscous friction losses, which are proportional to speed squared. This explains why dual-motor operation is preferred in this region. At lower speeds, however, the decrease in viscous friction losses does not outweigh the additional Joule losses in the second motor branch. It then becomes more interesting to only use one motor and to have the second torque delivered statically by a brake.

Another interesting observation is that the speed ratio never drops below zero. Referring to Fig. 3, $i < 0$ corresponds to a situation where one motor acts as a motor while the other works as a generator is not energy-efficient. Indeed: the internal power flow that arises only leads to additional energy losses [34]. Hence, as far as steady state operation is concerned, this type of operation should be avoided.

Finally, it can be noted that, in design 4, the sun brake is only used in a very limited region. In order to save weight, it can be left out of the design, with only a minimal loss of efficiency.

5. Experimental validation

5.1. Test setup

Fig. 6 shows the test setup that is used to study the actuator concept experimentally. The DMA is constructed using off-the shelf components. The planetary differential consists of a commercial Neugart PLFE 064 planetary gearbox (η_{PG}=94%) with a reduction ratio of 10:1. Instead of fixing the casing of the gearbox to the structure, a ball bearing is used to constrain the gearbox radially, while allowing it to rotate around its axis. Additionally, a spur gear is mounted on the casing (i.e., the ring), which is driven by the ring drivetrain through a 3:1 reduction. In this way, a planetary differential as depicted in Fig. 1 is created. The ring drivetrain is a 90W Maxon RE35 motor with a 73.5:1 Maxon GP42C gearbox (η_R=72%); the sun drivetrain is a 150W Maxon RE40 motor with 15:1 Maxon GP42C gearbox (η_R=81%). This design is equivalent to design 4 in Table 3, except for the ring gear ratio n_R. The overall ring reduction is thus 220.5:1, which is close to the 216:1 reduction specified in Table 3. Both motors are equipped with Maxon AB24 holding brakes (24V, 0.4Nm).

A 250W Maxon RE65 motor with 51:1 Maxon GP81A gearbox, which served as the reference drivetrain in section 4, is coupled to the DMA with an ETH Messtechnik DRBK-50 torque sensor in between, so that the torque provided by the drivetrains can be measured. The positions and speeds are obtained from Maxon HEDL 5540 encoders (500 CPT) mounted on each of the motors. A Maxon EPOS3 70/10 controller in Cyclic Synchronous Torque Mode imposes a constant torque on the 250W motor. A constant speed is imposed on the DMA's ring motor (by means of a Maxon MAXPOS 50/5) and sun motor (by means of a Maxon EPOS3 70/10). Both controllers are programmed in Cyclic Synchronous Velocity Mode, which uses a cascaded controller consisting of a high-frequency PI current loop and a low-frequency PI speed loop with acceleration and speed

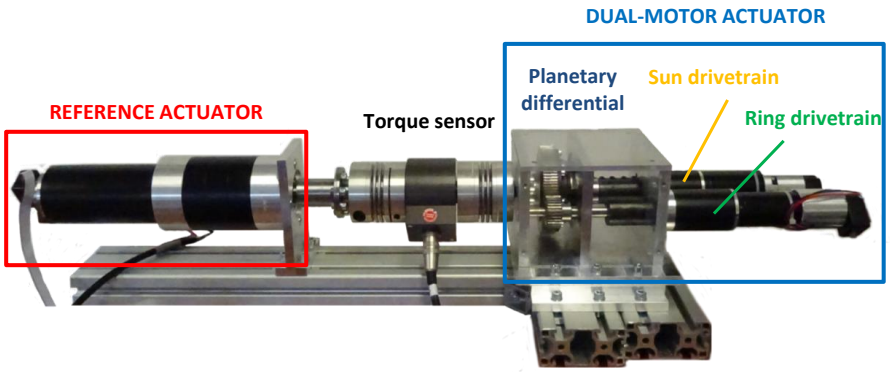

(a)

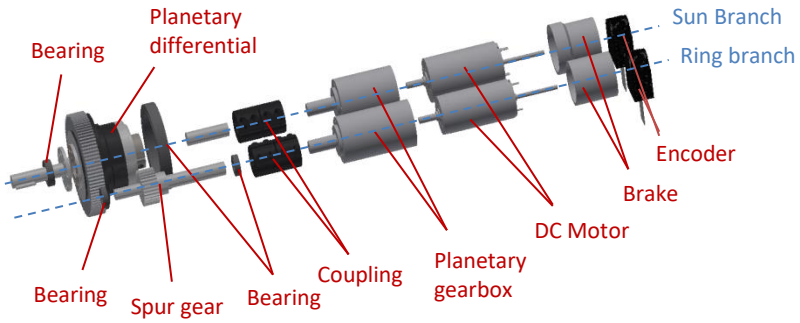

(b)

Figure 6: (a) Test setup used to validate the case study presented in section 4. The reference drivetrain (left) and the dual-motor actuator (right), designed with the intention of covering the same operating range as the reference motor, are coupled back-to-back with a torque sensor in between. (b) Exploded view of the dual-motor actuator.

feedforward. The controller relies on feedback from the encoders on the two motors of the DMA, i.e., there is no direct feedback from the output.

The Maxon AB24 holding brakes are normally engaged; they are disengaged by applying a voltage of 24V to the terminals. A Panasonic AQZ202 solid state relay is used to switch between the on and off state. It receives the switching command from a digital output of the MAXPOS or EPOS3 controller. The motor currents are retrieved from the EPOS3 and MAXPOS controllers, while the voltage at the motor terminals is obtained from a custom-made differential amplifier circuit board. The available sensors thus allow for a direct measurement of the mechanical and electrical power consumption of the actuators.

In order to determine the optimal operating mode of the DMA, three experiments were performed: one with a locked ring, one with a locked sun, and one

in dual-motor operation. In dual-motor operation, the optimal speed ratio was first determined experimentally by performing a slow (3-minute) sweep over a realistic range of speed ratios. In the actual experiment, constant speeds were imposed on both motors according to the speed ratio which yielded the lowest energy consumption during the sweep. The experimental energy consumptions presented below are the lowest among the three experiments.

5.2. Validation of the theoretical model

The model described in section 2 contains many a priori unknown friction coefficients. With the available experimental data, however, we can estimate these unknown coefficients.

Efficiency of planetary differential η_{PG}	88 %
Efficiency of sun gearbox η_S	81 %
Efficiency of ring gearbox η_R	66 %
Sun drivetrain viscous friction coefficient ν_S	1.5E-5 Nm/(rad/s)
Ring drivetrain viscous friction coefficient ν_R	2.1E-13 Nm/(rad/s)
Carrier viscous friction ν_C	2.9E-3 Nm/(rad/s)
Coulomb friction of sun drivetrain T_{CS}	0.0096 Nm
Coulomb friction of ring drivetrain T_{CR}	0.0049 Nm
Coulomb friction of carrier T_{CC}	0.091 Nm

Table 5: Empirical friction coefficients for the DMA design.

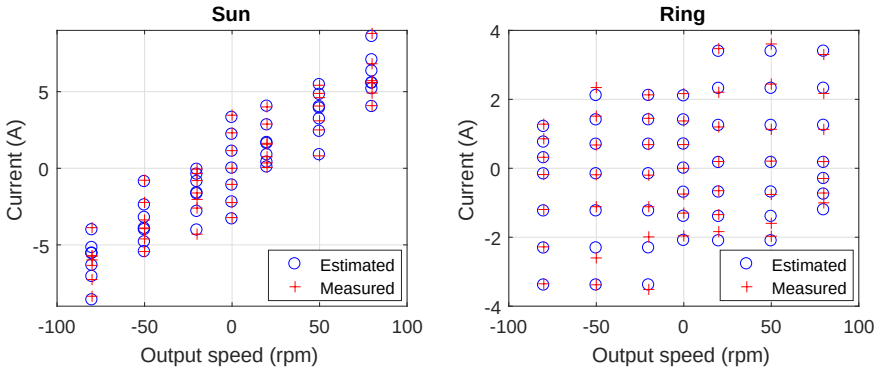

Figure 7: Currents obtained from experiments and the theoretical model, for various operating points. There is a good correspondence between the model and the measurements.

We imposed output torques of [-15,-10,-5,0,5,10,15] Nm at output speeds of [-80,-50,-20,0,20,50,80] rpm and calculated the expected currents based on Eq. (31) with the imposed speed and torque as input. These values were then fitted onto the motor current measurements, with the friction coefficients $T_{C\gamma}$, ν_γ ($\gamma = R, S$,C), η_S, η_R and η_{PG} as fitting parameters. The resulting parameters are listed in Table 5 and the fit is shown in Fig. 7. Overall, there is a good

Gearbox efficiency η_{ref}	87 %
Viscous friction coefficient ν_{ref}	2.05e-4 Nm/(rad/s)
Coulomb friction coefficient T_{Cref}	0.066 Nm

Table 6: Empirical friction coefficients for the reference drivetrain.

match between the measurements and the fitted model. The results therefore indicate that the model proposed in section 2 can be considered adequate.

A semi-empirical model of the reference drivetrain was obtained with the same procedure. The fitted equation for the current is

$$I_{ref} = \frac{1}{k_{t,ref}} \left[T_{Cref} sign\left(\omega_o\right) + \nu_{ref} \omega_o n_{ref} + \frac{C_{ref}}{n_{ref}} T_o \right] \tag{49}$$

with C_{ref} the gearbox efficiency function defined by Eq. 26. The fitted coefficients are listed in Table 6. The fitted gearbox efficiency (87%) is higher than the catalog efficiency (70%), indicating that gearbox losses for the reference drivetrain are better represented by Coulomb friction, as suggested by some other authors [32, 35, 36].

5.3. Power consumption

First, we would like to verify whether the DMA actually succeeds in reducing the energy consumption compared to the 250 W geared DC motor. To do so, we imposed a range of speeds and torques within the operating ranges of the actuators. The speed ratio was then hand-tuned to its optimal value for each measurement, following the procedure described earlier. Fig. 8 shows the experimentally obtained electrical power consumption for speeds of -20, 20, -50 and 50 rpm, for various torques within the actuator's operating range.

For most of the torque range, the DMA is indeed more efficient than the reference motor. The electrical energy consumption of the DMA does, however, increase more rapidly with torque. Figure 9, which shows the difference ΔP_{elec} between the energy consumption of the DMA and that of the reference drivetrain, indicates that the reference actuator actually becomes slightly more efficient for high torques. At low torques, however, the DMA is considerably more advantageous: at no-load at $\pm$50 rpm, it consumes up to 25 W less than the reference drive. At low speeds ($\pm$20 rpm), the difference is smaller, but there is still a 5 W reduction at no-load..

Also note that the plots in Figure 9 are asymmetrical around $T_o = 0$. Compared to the reference, the DMA tends to be relatively more efficient in reverse drive (positive torques at negative speeds or negative torques at positive speeds) than in forward drive (positive torques at positive speeds or negative torques at negative speeds).

5.4. Efficiency maps

The efficiency maps of the DMA and the reference drivetrain can be recalculated with the semi-empirical model. The results are shown in Fig. 10.

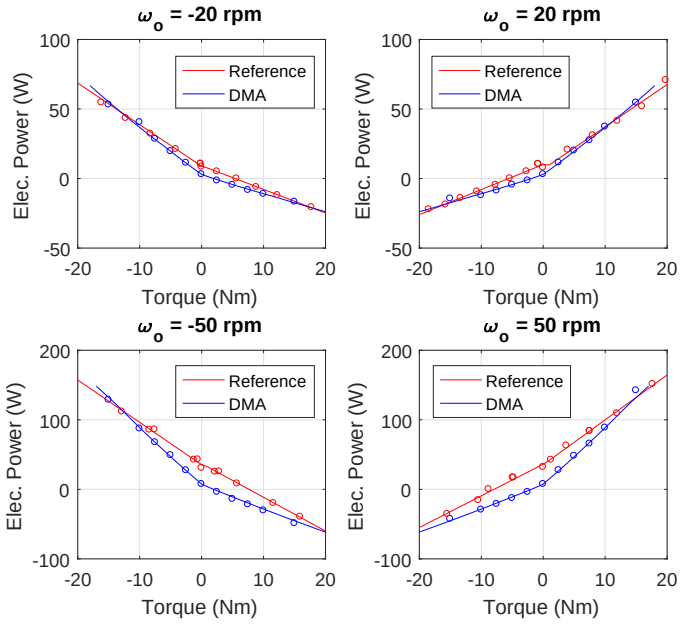

Figure 8: Power consumption of the dual-motor actuator and the reference motor, for a range of constant speeds and torques. Circles represent measured values, while the lines correspond to the fitted model defined by Eq. (49) (reference) or the full model from section 2.2 (DMA). The dual-motor actuator consumes less energy than the reference motor at low and moderate torques, especially at high speeds.

Comparing the efficiency maps to the theoretical ones (Fig. 4a and c), there is a clear difference in the size and shape of the zero-efficiency regions at low torques. For the DMA, it now stretches from 0 to ± 2 Nm at low speeds, where Coulomb friction dominates. At higher speeds, where viscous friction becomes more prominent, the zero-efficiency region continues up to torques of 4 Nm. The zero-efficiency region of the reference drivetrain experiences an even greater increase in size: it now ranges from 0 to ± 10 Nm at the maximum speed of 107 rpm.

The change in size and shape can be explained by Coulomb friction, which was included in the empirical model, but not in the simplified model from section 4. In addition to viscous friction losses, motors also suffer hysteresis losses (sometimes called remagnetization losses) which are proportional to speed, just like Coulomb friction losses [37]. Furthermore, gearboxes have a lower efficiency when used at low torques, something which is not accounted for in this paper. The torque-dependency of gearbox losses, too, can be represented by a Coulomb friction term [32, 35, 36]. Finally, additional bearings are required for the DMA; the friction in bearings presents itself mostly as Coulomb friction.

The increased size of the zero-efficiency regions has an impact on the average

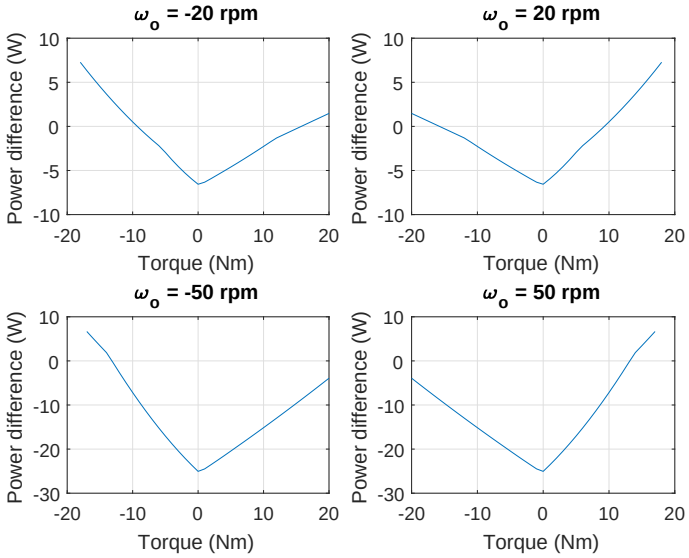

Figure 9: Difference in power consumption $\Delta P_{elec} = P_{elec,DMA} - P_{elec,ref}$ of the dual-motor actuator and the reference motor, for a range of constant speeds and torques. $P_{elec,DMA}$ and $P_{elec,ref}$ were obtained from a fit on the measurements. Except at the highest torques, the dual-motor actuator consumes less energy than the reference motor. The difference increases at high speeds.

efficiency of the actuators. The average efficiency of the reference drivetrain is DMA is 45%, slightly lower than the 51% in Table 3. The average efficiency of the DMA has decreased even more: the experimental value is 50%, which is 13% lower than the value predicted earlier (Table 3, design 4). This relatively larger decrease can, again, be traced down to the additional bearings in the DMA. There is, however, room for improvement: with a more integrated design, some of the bearings can be removed, and efficiency can be expected to increase.

In terms of maximum efficiency, the reference drivetrain (66%) performs better than the DMA (60%). This is in line with Figs. 8-9 where, at the highest torques, the DMA's energy consumption appeared to be higher than that of the reference drivetrain.

5.5. Optimal speed ratio

Based on the improved model with empirically-defined friction coefficients, we can also find the real optimal speed ratios for the actuator. This is done by performing a parameter sweep on i. The resulting speed ratios and operating modes are shown in Fig. 11.

The differences with the tentative catalog-based model, of which the results were presented in Fig. 5, are considerable. In comparison with the simulated results in Fig. 5b, the sun brake is used much more extensively. Furthermore, dual-motor operation is limited to those operating points that cannot be reached

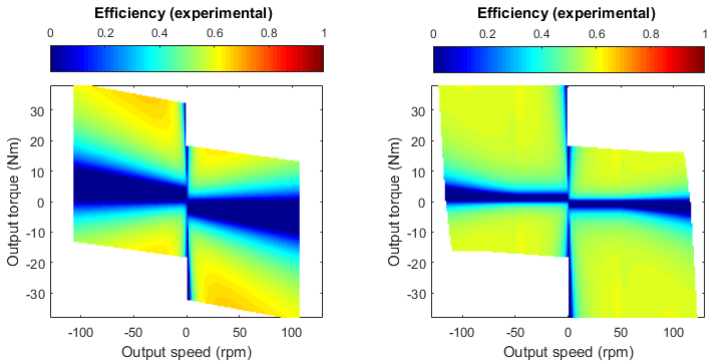

(a) Reference drivetrain. (b) DMA.

Figure 10: Efficiency maps based on the empirical models of the actuator. Although the maximum efficiency of the reference actuator is higher, the DMA is much more efficient at low speeds.

with a single motor. This can be explained by the friction from additional drivetrain components.

Recall that, in the theoretical model, the friction in the ring and sun branch was modeled as viscous friction. Friction coefficients derived from catalog information turned out to be of a similar order of magnitude. Conversely, the actual friction coefficients, listed in Table 5, are very different. According to Table 5, the experimentally determined Coulomb friction in the sun branch is twice as high as in the ring branch. The difference in viscous friction is even greater: it is eight orders of magnitude higher in the sun branch. The high friction losses in the sun branch explain why it is used almost exclusively when then ring branch cannot deliver the required output speed alone, and dual-motor operation is required. The ring branch is locked only at the highest torques, where Joule losses dominate. This is explained by the fact that the sun branch, according to Eq. (24), bears less torque, and the winding resistance of the motor is lower (see Table 2). Consequently, the sun motor experiences less Joule losses, and single-motor operation with locked ring is the preferred mode of operation at high-torque working points. Also note that the speed ratios in the dual-motor region are much higher than in Fig. 5. This means that, here too, the ring motor is used more extensively in order to reduce the impact of friction losses in the sun branch.

6. Discussion

The simulations and experiments in this work indicate that the proposed dual-motor actuation concept allows for a reduction of energy consumption over a traditional single-motor actuator. We showed that the operation of the actuator can be described entirely by a single parameter: the speed ratio i. Speed

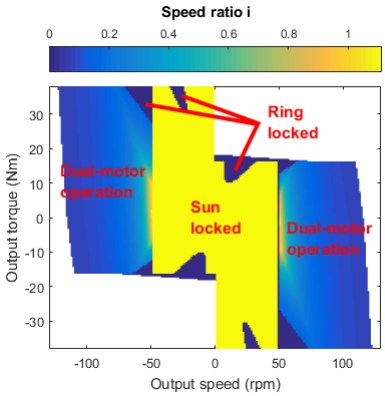

Figure 11: Optimal operating modes and speed ratio, based on the empirical model of the tested actuator. Dark blue denotes single-motor operation with locked ring; yellow denotes single-motor operation with locked sun; white denotes combinations of output speed and torque which violate the constraints listed in section 2.3. In dual-motor operation, the speed ratio is shown. This figure demonstrates that, in the presence of Coulomb friction and/or low gearbox efficiencies, single-motor operation should be exploited as much as possible.

ratios lower than zero correspond to a situation where one motor is delivering more power than needed by the load. The excess power is then absorbed by the other motor. The internal power flow in this type of operation causes unnecessary losses, leading us to conclude that speed ratios below zero should be avoided.

An important contribution of this work is the simple but detailed model of the actuator. We have shown that a good model is crucial for the selection of the optimal speed ratio and for deciding when to use the brakes. An important finding is that the results depend strongly on the amount of viscous and Coulomb friction and the way they are distributed over the branches. This was not discovered in previous research, where friction was systematically neglected to simplify the analysis. Unfortunately, very little information about these losses is provided in the manufacturers' catalogs. With efficiency values alone, the losses cannot be decomposed into viscous and Coulomb friction. Furthermore, energy losses calculated from datasheet information can differ greatly from the actual values [38]. For these reasons, an experimental characterization of the motors and gearboxes used in the prototype is crucial for the energy-optimal design and control of the actuator.

In our experiments, an approach where single-motor operation is maximized turned out to be the most energy-efficient solution. In this case, the sun branch, which exhibited high friction, would be locked at most operating points, while the ring branch (lower gearbox and motor efficiency) is locked at the highest torques. When viscous friction is high in both branches, however, dual-motor operation could be a better strategy at high speeds. These results strongly differed from those obtained with purely catalog-based models only, demonstrating that simplified optimization procedures based on catalog information, as well

as common cost functions such as T^2 or $(T\omega)^2$, are too simplistic to deliver the optimal speed ratio for dual-motor actuators. Instead, we suggest an approach where the actuator is characterized by fitting an adequate model onto measurements. From this model, which includes friction, optimal speed ratios can then be calculated with existing optimization methods. The result is an optimal speed ratio map, which can be used as a reliable input for the implementation of a controller.

The energetic benefits that a dual-motor actuator brings have to be assessed against its main disadvantage compared to a single-motor alternative: the fact that it consists of more components. This entails additional costs, a more complex design and assembly, and the need for additional drives and a more advanced control algorithm. Our results however indicate that the effective use of its composing drivetrains allows the dual-motor actuator to be competitive with single-motor alternatives in terms of weight and volume. This is an important consideration for mobile robots, where the energetic cost of the robot is directly influenced by its weight, and for wearable robots, where actuators need to be as compact as possible. In fact, efficiency, weight and size often overshadow the cost aspect in emerging fields such as assistive exoskeletons and powered prostheses [39]. The advantages can be even greater if the working range of the actuator can be shaped to the application – something which is possible with the dual-motor actuator. Hence, we believe that multi-motor concepts have a lot of potential in these fields.

On a final note, we would like to remark that the results in this work are limited to steady state operation. In applications with rapidly changing speeds or loads, internal dynamics come into play, possibly altering some of the conclusions drawn in this work. Future work will therefore focus on developing strategies to exploit dual-motor actuators in dynamic applications.

7. Conclusion

In this work, we presented a dual-motor actuation concept with a planetary differential and holding brakes. This actuator is potentially more efficient than a conventional motor-gearbox solution because of two reasons. First, the actuator has a redundant kinematic degree of freedom, meaning that output speed is a weighted sum of the two motor speeds. This redundancy can be exploited by distributing the speeds in such a way that the overall efficiency of the actuator is the highest. A second option is to use the holding brakes to lock one of the two branches. In this case, the locked branch no longer contributes to the output speed, but the losses in this branch are also completely eliminated. What we end up with by using the brakes, is equivalent to an actuator which can be sized to the operating point, and is therefore more efficient.

The control and design of the dual-motor actuator is, however, very sensitive to the speed- and load-dependent losses in the two drivetrains. Unfortunately, specific information about these losses is rarely available for off-the-shelf components. Experimental characterization should therefore be considered as an important step in the conception of energy-efficient dual-motor actuators.

Acknowledgment

Tom Verstraten is a PhD Fellow of the Research Foundation Flanders - Fonds voor Wetenschappelijk Onderzoek (FWO). David Rodriguez-Cianca is an SB Fellow of the same organization. This work has been partially funded by the European Commission starting grant SPEAR (grant no. 337596).

References

[1] T. Verstraten, G. Mathijssen, R. Furnémont, B. Vanderborght, and D. Lefeber, "Modeling and design of geared DC motors for energy efficiency: Comparison between theory and experiments," *Mechatronics*, vol. 30, pp. 198 – 213, 2015.

[2] W. Brown and A. Ulsoy, "A passive-assist design approach for improved reliability and efficiency of robot arms," in *Robotics and Automation (ICRA), 2011 IEEE International Conference on*, May 2011, pp. 4927–4934.

[3] C. Everarts, B. Dehez, and R. Ronsse, "Variable stiffness actuator applied to an active ankle prosthesis: Principle, energy-efficiency, and control," in *Intelligent Robots and Systems (IROS), 2012 IEEE/RSJ International Conference on*, Oct 2012, pp. 323–328.

[4] T. G. Sugar and M. Holgate, "Compliant mechanisms for robotic ankles," in *ASME 2013 International Design Engineering Technical Conferences and Computers and Information in Engineering Conference*. American Society of Mechanical Engineers, 2013, pp. V06AT07A002–V06AT07A002.

[5] S. Stramigioli, G. van Oort, and E. Dertien, "A concept for a new energy efficient actuator," in *Advanced Intelligent Mechatronics, 2008. AIM 2008. IEEE/ASME International Conference on*, July 2008, pp. 671–675.

[6] L. Mooney and H. Herr, "Continuously-variable series-elastic actuator," in *IEEE International Conference on Rehabilitation Robotics*, 2013.

[7] D. Dresscher, T. J. A. de Vries, and S. Stramigioli, "Inertia-driven controlled passive actuation," in *ASME 2015 Dynamic Systems and Control Conference*, no. 57267, 2015, pp. V003T45A002–.

[8] R. Aló, F. Bottiglione, and G. Mantriota, "An innovative design of artificial knee joint actuator with energy recovery capabilities," *Journal of Mechanisms and Robotics*, vol. 8, no. 1, pp. 011 009–011 009, Aug. 2015.

[9] B. Vanderborght, A. Albu-Schaeffer, A. Bicchi, E. Burdet, D. Caldwell, R. Carloni, M. Catalano, O. Eiberger, W. Friedl, G. Ganesh, M. Garabini, M. Grebenstein, G. Grioli, S. Haddadin, H. Hoppner, A. Jafari, M. Laffranchi, D. Lefeber, F. Petit, S. Stramigioli, N. Tsagarakis, M. V. Damme, R. V. Ham, L. Visser, and S. Wolf, "Variable impedance actuators: A review," *Robotics and Autonomous Systems*, vol. 61, no. 12, pp. 1601 – 1614, 2013.

[10] H. A. Y. Bonabi, M. N. Ahmadabadi, and F. Bahrami, "Distributed series elastic actuator: Analysis and simulations," in *2012 12th International Conference on Control, Automation and Systems*, Oct 2012, pp. 1949–1954.

[11] L. R. Ramelan, E. Firmansyah, T. H. Liu, S. K. Tseng, and J. W. Hsu, "An improved maximum efficiency control for dual-motor drive systems," in *2014 6th International Conference on Information Technology and Electrical Engineering (ICITEE)*, Oct 2014, pp. 1–6.

[12] S. K. Tseng, C. C. Tseng, T. H. Liu, and J. L. Chen, "Wide-range adjustable speed control method for dual-motor drive systems," *IET Electric Power Applications*, vol. 9, no. 2, pp. 107–116, 2015.

[13] W. Roozing, Z. Li, D. G. Caldwell, and N. G. Tsagarakis, "Design optimisation and control of compliant actuation arrangements in articulated robots for improved energy efficiency," *IEEE Robotics and Automation Letters*, vol. 1, no. 2, pp. 1110–1117, July 2016.

[14] G. Mathijssen, R. Furnémont, T. Verstraten, B. Brackx, J. Premec, R. Jiménez, D. Lefeber, and B. Vanderborght, "+SPEA introduction: Drastic actuator energy requirement reduction by symbiosis of parallel motors, springs and locking mechanisms," in *2016 IEEE International Conference on Robotics and Automation (ICRA)*, May 2016, pp. 676–681.

[15] J. B. Morrell and J. K. Salisbury, "Parallel-coupled micro-macro actuators," *The International Journal of Robotics Research*, vol. 17, no. 7, pp. 773–791, 1998.

[16] M. Zinn, B. Roth, O. Khatib, and J. K. Salisbury, "A new actuation approach for human friendly robot design," *The International Journal of Robotics Research*, vol. 23, no. 4-5, pp. 379–398, 2004.

[17] J. Ontañón Ruiz, R. W. Daniel, and P. R. McĂree, "On the use of differential drives for overcoming transmission nonlinearities," *Journal of Robotic Systems*, vol. 15, no. 11, pp. 641–660, 1998.

[18] B.-S. Kim, J.-J. Park, and J.-B. Song, "Improved manipulation efficiency using a serial-type dual actuator unit," in *Control, Automation and Systems, 2007. ICCAS '07. International Conference on*, Oct 2007, pp. 30–35.

[19] B. S. Kim, J. B. Song, and J. J. Park, "A serial-type dual actuator unit with planetary gear train: Basic design and applications," *IEEE/ASME Transactions on Mechatronics*, vol. 15, no. 1, pp. 108–116, Feb 2010.

[20] H. Lee and Y. Choi, "A new actuator system using dual-motors and a planetary gear," *IEEE/ASME Transactions on Mechatronics*, vol. 17, no. 1, pp. 192–197, Feb 2012.

[21] A. Girard and H. H. Asada, "A two-speed actuator for robotics with fast seamless gear shifting," in *Intelligent Robots and Systems (IROS), 2015 IEEE/RSJ International Conference on*, Sept 2015, pp. 4704–4711.

[22] ——, "A practical optimal control approach for two-speed actuators," in *2016 IEEE International Conference on Robotics and Automation (ICRA)*, May 2016, pp. 4572–4577.

[23] ——, "Leveraging natural load dynamics with variable gear-ratio actuators," *IEEE Robotics and Automation Letters*, vol. 2, no. 2, pp. 741–748, April 2017.

[24] V. Babin, C. Gosselin, and J.-F. Allan, "A dual-motor robot joint mechanism with epicyclic gear train," in *Intelligent Robots and Systems (IROS 2014), 2014 IEEE/RSJ International Conference on*, Sept 2014, pp. 472–477.

[25] P. Gao, A. Ren, and W. Zong, "Study on a variable stiffness actuation with differential drives," in *2016 IEEE International Conference on Cyber Technology in Automation, Control, and Intelligent Systems (CYBER)*, June 2016, pp. 249–254.

[26] D. Y. Goswami, *The CRC handbook of mechanical engineering*. CRC press, 2014.

[27] H. W. Müller, *Epicyclic drive trains: Analysis, synthesis, and applications*, J. Glover, Ed. Wayne State University Press, 1982.

[28] D. W. McKinley and J. K. Parmerlee, "Bi-stable brake," U.S. Patent 3,741,353, Jun. 26, 1973.

[29] M. Plooij, T. van der Hoeven, G. Dunning, and M. Wisse, "Statically balanced brakes," *Precision Engineering*, vol. 43, no. Supplement C, pp. 468 – 478, 2016.

[30] S. Diller, C. Majidi, and S. H. Collins, "A lightweight, low-power electroadhesive clutch and spring for exoskeleton actuation," in *2016 IEEE International Conference on Robotics and Automation (ICRA)*, May 2016, pp. 682–689.

[31] S. Dereyne, P. Defreyne, E. Algoet, S. Derammelaere, and K. Stockman, "Efficiency measurement campaign on gearboxes," in *Energy Efficiency in Motor Driven Systems (EEMODS), 2015 International Conference on*, 2015.

[32] C. Pelchen, C. Schweiger, and M. Otter, "Modeling and simulating the efficiency of gearboxes and of planetary gearboxes," in *Proceedings of 2nd International Modelica Conference*, 2002, pp. 257–266.

[33] T. Verstraten, R. Furnémont, G. Mathijssen, B. Vanderborght, and D. Lefeber, "Energy consumption of geared DC motors in dynamic applications: Comparing modeling approaches," *IEEE Robotics and Automation Letters*, vol. 1, no. 1, pp. 524–530, 2016.

[34] A. Abate, J. W. Hurst, and R. L. Hatton, "Mechanical antagonism in legged robots," in *Robotics: Science and Systems*, 2016.

[35] D. Dresscher, T. J. A. de Vries, and S. Stramigioli, "Motor-gearbox selection for energy efficiency," in *2016 IEEE International Conference on Advanced Intelligent Mechatronics (AIM)*, July 2016, pp. 669–675.

[36] S. Seok, A. Wang, M. Y. Chuah, D. Otten, J. Lang, and S. Kim, "Design principles for highly efficient quadrupeds and implementation on the MIT Cheetah robot," in *Robotics and Automation (ICRA), 2013 IEEE International Conference on*, May 2013, pp. 3307–3312.

[37] J. Gieras, *Permanent Magnet Motor Technology: Design and Applications*, ser. Electrical and Computer Engineering. Taylor & Francis, 2011. [Online]. Available: http://books.google.be/books?id=rFrFLUTri0MC

[38] S. Derammelaere, S. Dereyne, P. Defreyne, E. Algoet, F. Verbelen, and K. Stockman, "Energy efficiency measurement procedure for gearboxes in their entire operating range," in *2014 IEEE Industry Application Society Annual Meeting*, Oct 2014, pp. 1–9.

[39] A. J. Veale and S. Q. Xie, "Towards compliant and wearable robotic orthoses: A review of current and emerging actuator technologies," *Medical Engineering & Physics*, vol. 38, no. 4, pp. 317 – 325, 2016.